

Searching for Magnetic Monopoles with Earth's Magnetic Field

Yang Bai¹, Sida Lu², and Nicholas Orlofsky³

¹*Department of Physics, University of Wisconsin-Madison, Madison, Wisconsin 53706, USA*

²*Department of Physics, Tel Aviv University, Tel-Aviv 69978, Israel*

³*Department of Physics, Carleton University, Ottawa, Ontario K1S 5B6, Canada*

 (Received 28 April 2021; accepted 10 August 2021; published 31 August 2021)

Magnetic monopoles have long been predicted in theory and could exist as a stable object in our Universe. As they move around in galaxies, magnetic monopoles could be captured by astrophysical objects like stars and planets. Here, we provide a novel method to search for magnetic monopoles by detecting the monopole moment of Earth's magnetic field. Using over six years of public geomagnetic field data obtained by the *Swarm* satellites, we apply Gauss's law to measure the total magnetic flux, which is proportional to the total magnetic charge inside Earth. To account for the secular variation of satellite altitudes, we define an altitude-rescaled magnetic flux to reduce the dominant magnetic dipole contribution. The measured magnetic flux is consistent with the existing magnetic field model that does not contain a monopole moment term. We therefore set an upper limit on the magnetic field strength at Earth's surface from magnetic monopoles to be $|B_m| < 0.13$ nT at 95% confidence level, which is less than 2×10^{-6} of Earth's magnetic field strength. This constrains the abundance of magnetically charged objects, including magnetic black holes with large magnetic charges.

DOI: 10.1103/PhysRevLett.127.101801

Introduction.—As proposed by Dirac close to a century ago [1], the magnetic monopole is a fascinating physical object that could elegantly explain the quantization of electric charges in nature. Ever since, physicists have been studying magnetic monopoles both from theoretical and experimental directions. On the theory side, the discovery of Polyakov–'t Hooft monopoles in 1974 [2,3] has been applied to grand unified theories (GUTs) [4], which predict the GUT monopole mass around 10^{17} GeV. Lighter masses near the electroweak scale have also been proposed and searched for [5–7]. For heavier masses above the Planck mass scale, magnetically charged black holes have long been proposed, which can have masses proportional to their magnetic charges [8–10]. Various experimental methods have been adopted to search for magnetic monopoles, e.g., detecting the quantized jump in magnetic flux when monopoles pass a superconducting quantum interference device [11] and searching for the Cherenkov light generated when the accelerated monopoles pass the large IceCube detector [12]. Magnetic monopoles could also be captured by stars and planets including our Earth, and their annihilations can produce detectable neutrinos and/or heat [13–15] (see also [15–18] for further constraints).

In this Letter, we present a new way to search for magnetic monopoles by measuring the magnetic monopole moment of Earth.

Ever since the classical 1839 paper by Gauss [19] (see [20] for English translation), measurements indicate Earth's magnetic field is dominantly dipolelike with subleading contributions from higher moments. Although the general spherical harmonics formula developed by Gauss contains the monopole moment [19], it has been assumed to be zero because the traditional Maxwell equations lack magnetically charged objects.

To measure different magnetic moments, including the monopole moment of Earth, one could perform a global fit like the one used for the International Geomagnetic Reference Field [21]. In this Letter, we adopt a simpler approach and apply Gauss's law to Earth's magnetic field to obtain the total magnetic flux, proportional to the enclosed magnetic charge. We analyze the more than six years of publicly available data by the European Space Agency *Swarm* mission [22,23], which consists of three satellites in low-Earth near-polar orbits measuring the vector magnetic field.

Measuring the monopole moment.—For a single object or a group of objects with a total magnetic charge of Q at the center of Earth, Earth's magnetic field has a monopole moment of $\mathbf{B}_m(\mathbf{r}) = [(Qg)/4\pi r^2]\hat{\mathbf{r}} = (Q/2er^2)\hat{\mathbf{r}}$, where $e = \sqrt{4\pi\alpha}$ with $\alpha \approx 1/137$ as the fine-structure constant and $g = 2\pi/e \approx 68.5e \approx 21$ is the magnetic coupling. For equations, we use natural units with $\hbar = c = \epsilon_0 = 1$, although numerical values are expressed in the International System

Published by the American Physical Society under the terms of the Creative Commons Attribution 4.0 International license. Further distribution of this work must maintain attribution to the author(s) and the published article's title, journal citation, and DOI. Funded by SCOAP³.

of Units. $Q = 1$ is the minimal magnetic charge, corresponding to the Dirac quantization condition with $eg = 2\pi$ [1]. Numerically, $B_m \approx 0.082 \text{ nT} \times (R_\oplus/r)^2 (Q/10^{19})$, where $R_\oplus \approx 6371.2 \text{ km}$ is the average radius of Earth. For comparison, the measured Earth surface intensity has a magnitude of up to $\approx 65000 \text{ nT}$.

To measure the magnetic charge, one could adopt Gauss's law $\oint \mathbf{B}(\mathbf{r}) \cdot d\mathbf{A} = Qg$. This requires a full-sky measurement of the magnetic vector field. For convenience, one could choose the manifold to be a sphere of radius R centered on Earth. Then, $d\mathbf{A} = R^2 \hat{\mathbf{n}} d\Omega$ with $\hat{\mathbf{n}}$ as a unit surface vector pointing outward and $d\Omega = \sin\theta d\theta d\phi$ in spherical coordinates. For magnetic monopole objects, $\bar{B}_m \equiv (1/4\pi) \oint \mathbf{B}_m(r, \theta, \phi) \cdot \hat{\mathbf{n}} d\Omega = Qg(1/4\pi R^2)$. Here, we have defined a solid-angle averaged magnetic field \bar{B} , which is simply the amplitude of the monopole magnetic field at radius R . All higher multiple moments beyond \mathbf{B}_m do not contribute to \bar{B} .

In practice, the measurement of magnetic field is not performed at a uniform radius—the *Swarm* satellite orbits have a variation of $\mathcal{O}(1\%)$ during one orbit and decay over time. Thus, it is not possible to integrate the magnetic flux along a perfectly spherical closed manifold, and the surface's normal vector $\hat{\mathbf{n}}$ will not match the radial coordinate unit vector $\hat{\mathbf{r}}$. So, a numerical integration of $\int \mathbf{B}(r, \theta, \phi) \cdot \hat{\mathbf{r}} d\Omega$ will not be zero, even in the absence of a monopole term (for *Swarm*'s orbital parameters, $\bar{B} \simeq -70 \text{ nT}$, see the Supplemental Material [24]). To suppress this measurement-induced dipole contribution, we use the following modified Gauss law to measure the magnetic field from the monopole charge:

$$\bar{B} = \frac{1}{4\pi} \int \left[\frac{r(\theta, \phi)}{R_{\text{ref}}} \right]^3 \mathbf{B}(r, \theta, \phi) \cdot \hat{\mathbf{r}} d\Omega. \quad (1)$$

Here, $r(\theta, \phi)$ is the radius of the magnetic measurement at different angular directions and R_{ref} is a fixed reference radius. For the dipole component, this is formally equivalent to integrating on a perfectly spherical surface at $r = R_{\text{ref}}$, so $\hat{\mathbf{n}} = \hat{\mathbf{r}}$ and the dipole component contributes zero to the above quantity. Note that Earth's higher-moment magnetic fields have nonzero contributions to the quantity \bar{B} because the higher moments scale with higher powers of r . For instance, the quadrupole moment has a magnitude of $\mathcal{O}(10\%)$ of the dipole moment and contributes around 0.5 nT for \bar{B} using *Swarm*'s orbit. Therefore, the r^3 scaling in Eq. (1) is practically useful to improve the sensitivity of searching for the monopole moment because it reduces contributions to \bar{B} from the dipole and higher moments while preserving the monopole signal.

Data analysis.—We use the VirES architecture to access the data via the PYTHON package VIRESCIENT [25]. Magnetic field measurements are used from the *Swarm* L1b 1 Hz data product. When selecting data, we take the

following considerations. Because of a sensor failure in *Swarm C*, we only use the data from the other two satellites, *Swarm A* and *Swarm B*. Bad data are removed using the Flags_F filter, and only nonzero vector data for which the magnetic activity level $Kp \leq 3$ are included to reduce the impact of the Sun (following the procedure in Refs. [26,27]). Unlike other analyses, we do not impose a cut on the Sun's elevation angle above the horizon, as this would prevent us from obtaining full 4π sky coverage (particularly near the poles).

To calculate \bar{B} , the measurements are binned into $a \times a$ degree angular patches and d -day-long time bins. If the satellites do not cover all $a \times a$ degree patches within a given d -day time bin, that bin is not used. Because of the orbital inclinations (87.4° for *Swarm A* and 88° for *Swarm B*), the regions closest to the poles are never measured; therefore, the patches closest to the poles are imposed to have size $3^\circ(\text{latitude}) \times a^\circ(\text{longitude})$ when $a < 3$. We index the individual measurements, angular patches, and time bins by i, j , and k , respectively. To estimate the magnetic flux for a given time bin, we first rescale the measurements of the magnetic field in the radial direction B_r to a common radius $R_{\text{ref}} = 6850 \text{ km}$, the average radius of both satellites for the mission duration thus far, as $B_{r,i}(\theta_i, \phi_i) = B_{r,i}(r_i, \theta_i, \phi_i)(r_i/R_{\text{ref}})^3$. Then, we average every rescaled measurement of the magnetic field in the radial direction within each angular patch $\langle B_r \rangle_j = N_j^{-1} \sum_{i|(\theta_i, \phi_i) \in \text{patch } j} B_{r,i}(\theta_i, \phi_i)$, with N_j as the number of measurements in patch j . These patch averages are then summed together, weighted by the area of each patch, to obtain $\bar{B} = \sum_j \langle B_r \rangle_j w_j$, with $w_j = (4\pi)^{-1} \int_{\text{patch } j} \sin\theta d\theta d\phi$. To obtain an estimate of the statistical error, the squared standard error of the mean is calculated for each angular patch as $\sigma_j^2 = (N_j - 1)^{-1} N_j^{-1} \sum_{i|(\theta_i, \phi_i) \in \text{patch } j} [B_{r,i}(\theta_i, \phi_i) - \langle B_r \rangle_j]^2$. We have checked that the errors in each measurement, which are of order few nanotesla [26], are trivial compared to the errors from having different measurements at different positions and times within each patch. These errors are weighted summed in quadrature to obtain the squared error of the total flux $\sigma^2 = \sum_j \sigma_j^2 w_j^2$. For each time bin k , this procedure yields an estimate for \bar{B}_k and its statistical uncertainty σ_k . The error for each time bin scales as $\sigma_k \propto a$.

The approach outlined above contains several systematic errors, so \bar{B} cannot be identified with \bar{B} . These include the imperfect spherical coverage, which depends on the orbital path taken, the finite angular patch size used to numerically integrate (1), the finite time bin size when compared against the nonstatic nature of the fields, and the other magnetic field components besides the dominant dipole component that are not canceled using the r^3 rescaling in (1). On the other hand, the existence of a monopole moment will lead to a deviation between data and model, as the current models do not include the monopole term. Therefore, a

better quantity to analyze would be $\bar{B}_k^{\text{dif}} = \bar{B}_k^{\text{dat}} - \bar{B}_k^{\text{mod}}$, which reduces the systematic errors and manifests the deviation simultaneously. For each time bin k , we add the data and model uncertainties in quadrature $(\sigma_k^{\text{dif}})^2 = (\sigma_k^{\text{dat}})^2 + (\sigma_k^{\text{mod}})^2$, then average $\langle \bar{B}^{\text{dif}} \rangle = (\sigma^{\text{dif}})^2 \sum_k \bar{B}_k^{\text{dif}} / (\sigma_k^{\text{dif}})^2$. The squared error of $\langle \bar{B}^{\text{dif}} \rangle$ is $(\sigma^{\text{dif}})^2 = [\sum_k 1/(\sigma_k^{\text{dif}})^2]^{-1}$.

When the variation between time bins is larger than their statistical uncertainties would suggest, we enlarge the overall uncertainty by the Birge ratio [28,29] $r_B = \sqrt{\chi^2/(N_k - 1)}$ or $\sigma = \max[1, r_B] \sigma^{\text{dif}}$, with χ^2 the goodness of fit and N_k the number of time bins. When $r_B > 1$, this enlarged error is essentially equivalent to the standard error of the mean of $\langle \bar{B}^{\text{dif}} \rangle$, i.e., $(\sigma^{\text{sem}})^2 = (N_k - 1)^{-1} N_k^{-1} \sum_k (\bar{B}_k^{\text{dif}} - \langle \bar{B}^{\text{dif}} \rangle)^2$. Note, σ^{sem} is irreducible in the limit $a \rightarrow 0$ provided a is small enough for each time bin's measured \bar{B}_k^{dif} to stabilize numerically (but not so small that there are empty angular patches without measurements). It can be interpreted as including additional variability effects not included in the purely statistical error, including different orbital paths or acceptance cuts in each time bin [30].

Model prediction.—To provide a sense of how much each component of Earth's field contributes to our estimate of the flux, the various contributions are summarized in Table I, showing the prediction for $\langle \bar{B}^{\text{mod}} \rangle$ (the time average of the model alone) from various components of the CHAOS-7 model [27] using $a = 2$, $d = 180$, and $Kp \leq 3$ (see also the shaded bands in Fig. 1). The core component is separated into the dipole and higher moments. The second column shows the calculation under idealized conditions where all measurements are taken at the same time and on an equal-radius sphere, with (θ, ϕ) still matching the satellite measurements. These terms formally go to zero when $a \rightarrow 0$, so they can be interpreted as the systematic error from the discretization of the angular integral. The crust and external components contribute negligibly (see details in the Supplemental Material [24]).

The third column uses the actual variation in the satellite altitude and rescales the field by $(r/R_{\text{ref}})^3$ as in Eq. (1), but still removes time dependence. This shows the error introduced by the r^3 rescaling. Note, the dipole results match whether taken on a sphere or rescaled because the two operations are mathematically equivalent. The dipole dominates the full model's error because its overall contribution to the field is larger, and its value is consistent with zero. On the other hand, the higher core moments have much larger $\langle \bar{B}^{\text{mod}} \rangle$ when calculated at the satellite radius (compared with both the dipole and higher-moment calculation on sphere) because higher moments are proportional to r^{-n} with $n > 3$. Thus, higher moments provide the dominant contribution to $\langle \bar{B}^{\text{mod}} \rangle$. Unlike the on-sphere calculation, there is relatively little suppression of $\langle \bar{B}^{\text{mod}} \rangle$ as $a \rightarrow 0$ because of the saturated contribution from the higher moments when evaluated at the satellite radius. Finally, the last column shows that time dependence is a subdominant effect for most of the model components.

Results.—Values for a and d are chosen for numerical stability in the calculation of both $\langle \bar{B}^{\text{dif}} \rangle$ and its uncertainty and to obtain good agreement between all time bins and the average value. These tend to prefer larger d and smaller a , although a cannot be too small so that all angular patches are measured within each time bin. In general, as shown in the Supplemental Material [24], any value of a between 2 and 0.3 gives similar results for large enough d (with the requisite d increasing with decreasing a). They are also robust against the choice of Kp cut.

Using $a = 2$ and $d = 180$, the average difference between the data and model is $\langle \bar{B}^{\text{dif}} \rangle = 0.022 \pm 0.046$ nT, with a goodness of fit to the mean $\chi^2 = 16.2$ with $N_k - 1 = 12$ degrees of freedom. The quoted uncertainty has been marginally enhanced by the Birge factor from the purely statistical uncertainty of 0.039 nT. Full-sky coverage is obtained in each time bin. A plot of the measurements in each time bin for both data and model is shown in Fig. 1, along with the contributions from the dipole and higher moments individually. The data and model follow each

TABLE I. Values for the average flux $\langle \bar{B}^{\text{mod}} \rangle$ and its 1σ statistical error in nanotesla from various model components in the CHAOS-7 model [27] of Earth's magnetic field, evaluated along the satellites' trajectories and spanning the time period from February 1, 2014 to June 29, 2020. The second and third columns remove the model's time dependence and, respectively, assume either the measurements are taken on a sphere with fixed radius or at the satellite radii and rescaled by $(r/R_{\text{ref}})^3$ as in (1). The final column uses the satellite radii and includes the model's time dependence. Results are for $a = 2$, $d = 180$, and $Kp \leq 3$.

Model component	On sphere	At satellite radius	
	Same time	Same time	Time dependent
Lithosphere	$-0.000033(\pm 24)$	$-0.000087(\pm 26)$	$-0.000087(\pm 26)^a$
External	$-0.000088(\pm 66)$	0.013 ± 0.000008	0.022 ± 0.0001
Core dipole	0.032 ± 0.025	0.032 ± 0.025	0.030 ± 0.025
Core higher moments	-0.20 ± 0.01	-0.56 ± 0.01	-0.57 ± 0.01
Full model	-0.17 ± 0.03	-0.51 ± 0.03	-0.52 ± 0.03

^aThe lithosphere component is time independent by model assumption.

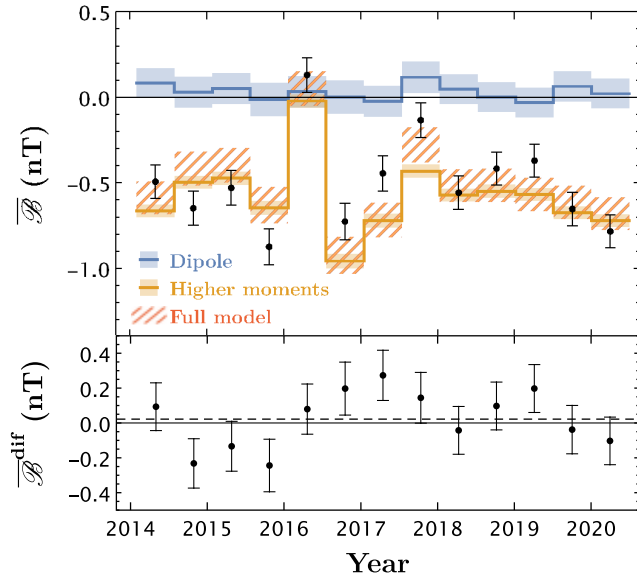


FIG. 1. Average value and error of \overline{B} in 180-day bins using 2° angular patch size covering the time period from February 1, 2014 to June 29, 2020. Data from *Swarm A* and *B* were incorporated, with the selection criteria $Kp \leq 3$. In the top panel, the blue and yellow lines indicate the contribution from the core's dipole and higher moments, respectively, to the model prediction, with the shaded bands giving their errors. The hatched regions show the total model predictions with errors. Data are shown by black points. In the lower panel, the differences between the data and model are shown, and the dashed line indicates the mean. All error bars are 1σ and include only statistical error.

other very closely. The model's value is dominated by the core's higher moments, but its uncertainty is dominated by the core's dipole moment because of the dipole's much larger overall contribution to the magnetic field. If a is decreased, as shown in the Supplemental Material [24], the statistical error bars for individual time bins shrink, but the overall error is dominated by the variation between time bins and levels off.

Because no significant difference between the data and model is found, we perform a signal injection (adding a monopole component into the model and increasing it until the model becomes incompatible with data) to set a bound on the magnitude of the monopole component field at 95% confidence level: $-0.07 < B_m(r = R_{\text{ref}}) < 0.11$ nT, in agreement with the 2σ range of $\langle \overline{B}^{\text{dif}} \rangle$. This translates into an upper bound on the monopole component field at Earth's surface $|B_m(r = R_\oplus)| < 0.13$ nT and on the net magnetic charge $|Q_{\text{net}}| < 1.6 \times 10^{19} \equiv Q_{\text{max}}$.

Constraints on magnetic monopole objects.—One can apply the constraints on the total net magnetic charge $|Q_{\text{net}}| < Q_{\text{max}}$ into various fundamental theories that predict magnetic monopole objects with different charge-to-mass ratios, which we parametrize by $q \equiv Q/Q_{\text{ext}}$ with $Q_{\text{ext}} = eM/[\cos(\theta_W)\sqrt{\pi}M_{\text{pl}}] \approx 0.19M/M_{\text{pl}}$. Here, Q_{ext} is the charge of an extremal magnetic black hole with an

electroweak symmetric corona of mass M [10,15], with $M_{\text{pl}} = 1.22 \times 10^{19}$ GeV/ c^2 as the Planck mass, θ_W as the weak mixing angle, and e as the electric coupling constant. A magnetic black hole has $q \leq 1$ (saturated to equality in the extremal limit) and $M > M_{\text{pl}}$. Because magnetic black holes can efficiently Hawking radiate into electrons if their temperature is sufficiently large, they satisfy $q \sim 1$ whenever $M \lesssim 10^{17}$ g [10,15,18], but can take on any $q \leq 1$ at larger masses. Conversely, a monopole particle has $q > 1$ according to the weak gravity conjecture [31]. While a GUT monopole with $Q = 2$ and mass $M \approx 10^{17}$ GeV/ c^2 has $q \approx 1300$, a gravitating composite monopole object with a large magnetic charge could have much larger mass with both small and large q [32]. Therefore, we treat q and M as free model parameters to set limits.

During Earth's lifetime, it will have captured $N \approx 3800f$ (10^{15} g/ M) monopoles, with $f = \rho/(0.4 \text{ GeV cm}^{-3})$ the local monopole energy density ρ as a fraction of the local dark matter density [15,33]. When $N \geq 1$, the net charge of captured monopoles is $Q_{\text{net}} \approx \sqrt{N}Q$. Thus, the constraint $|Q_{\text{net}}| < Q_{\text{max}}$ can be expressed as a limit on the local density of monopoles: $f \lesssim 8.8 \times 10^{-4}q^{-2}[Q_{\text{max}}/(1.6 \times 10^{19})]^2(10^{15} \text{ g}/M)$, valid in the regime

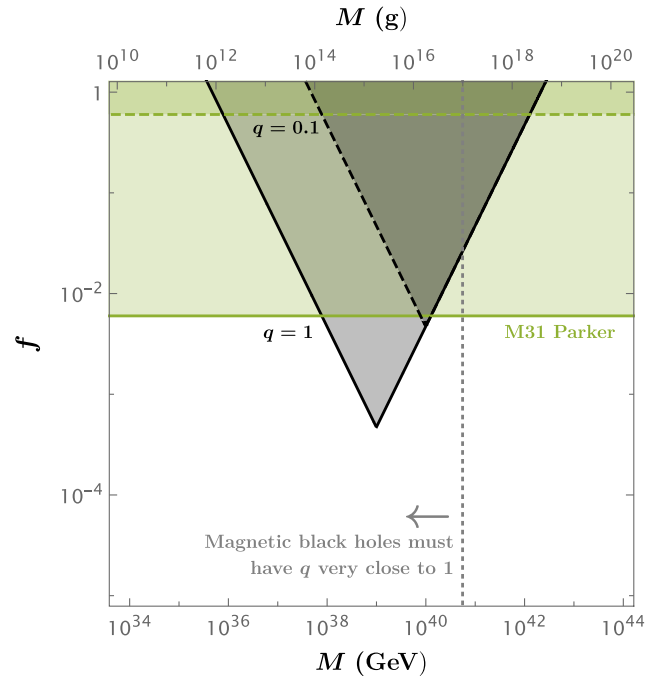


FIG. 2. Bounds on the local energy density of magnetic monopoles as a fraction of the local dark matter density. Black shaded area is the bound from Earth's magnetic monopole moment, bounding Earth's net magnetic charge by $Q_{\text{max}} = 1.6 \times 10^{19}$. Green is the M31 Parker bound [15]. Solid is $q = 1$, while dashed is $q = 0.1$. To the left of the gray dashed line, magnetic black holes must be close to the stable extremal state ($q \sim 1$), though other magnetically charged objects with different q could exist.

$f \gtrsim 2.6 \times 10^{-4}(M/(10^{15} \text{ g}))$. This is depicted in Fig. 2. Also shown is the Parker bound [34,35] derived from M31 in [15], $f \lesssim 6 \times 10^{-3}q^{-2}$, which disappears when $q < 0.08$. The limit presented here is complimentary to other limits—for example, from gas heating and white dwarf destruction [18]—in that it is a direct measurement as opposed to an inference from difficult-to-model astrophysical systems.

Discussion.—The Earth’s magnetic field provides an interesting way to search for new physics. Using satellite-based measurements, we have shown it is possible to estimate a bound on the magnetic flux with a modified version of Gauss’s law. Even without any knowledge of the higher multiple moments, the monopole moment can be constrained at the level of $\mathcal{O}(\text{nT})$ [the value for \vec{B} when r^3 rescaling as in (1) is employed], and comparing to a model of the higher moments allows for bounds an order of magnitude stronger. This suggests that future model fits should include the possibility of a monopole term. Combining a global fitting technique with data from more observatories would provide the best achievable bound with present technology. We encourage future work in this direction to build on the work presented here. Mars, which also has satellite-based measurements of its magnetic field [36], could be another interesting target for future work.

We thank Joshua Berger and Mrunal Korwar for useful discussion. The work of Y. B. is supported by the U.S. Department of Energy under Award No. DE-SC-0017647. The work of S. L. is supported in part by Israel Science Foundation under Grant No. 1302/19. The work of N. O. is supported by the Arthur B. McDonald Canadian Astroparticle Physics Research Institute.

-
- [1] P. A. M. Dirac, *Proc. R. Soc. A* **133**, 60 (1931).
 - [2] A. M. Polyakov, *JETP Lett.* **20**, 194 (1974), http://jetpletters.ru/ps/1789/article_27297.shtml.
 - [3] G. 't Hooft, *Nucl. Phys.* **B79**, 276 (1974).
 - [4] H. Georgi and S. Glashow, *Phys. Rev. Lett.* **32**, 438 (1974).
 - [5] Y. M. Cho and D. Maison, *Phys. Lett. B* **391**, 360 (1997).
 - [6] O. Gould and A. Rajantie, *Phys. Rev. Lett.* **119**, 241601 (2017).
 - [7] P. Q. Hung, *Nucl. Phys.* **B962**, 115278 (2021).
 - [8] K. Lee, V. P. Nair, and E. J. Weinberg, *Phys. Rev. Lett.* **68**, 1100 (1992).
 - [9] K. Lee, V. P. Nair, and E. J. Weinberg, *Phys. Rev. D* **45**, 2751 (1992).

- [10] J. Maldacena, *J. High Energy Phys.* **04** (2021) 079.
- [11] B. Cabrera, *Phys. Rev. Lett.* **48**, 1378 (1982).
- [12] M. G. Aartsen *et al.* (IceCube Collaboration), *Eur. Phys. J. C* **76**, 133 (2016).
- [13] R. A. Carrigan, *Nature (London)* **288**, 348 (1980).
- [14] J. A. Frieman, K. Freese, and M. S. Turner, *Astrophys. J.* **335**, 844 (1988).
- [15] Y. Bai, J. Berger, M. Korwar, and N. Orlofsky, *J. High Energy Phys.* **10** (2020) 210.
- [16] N. E. Mavromatos and V. A. Mitsou, *Int. J. Mod. Phys. A* **35**, 2030012 (2020).
- [17] D. Ghosh, A. Thalapillil, and F. Ullah, *Phys. Rev. D* **103**, 023006 (2021).
- [18] M. D. Diamond and D. E. Kaplan, [arXiv:2103.01850](https://arxiv.org/abs/2103.01850).
- [19] C. F. Gauss, *Allgemeine theorie des erdmagnetismus, in Werke: Fünfter Band* (Springer, Berlin, Heidelberg, 1877), pp. 119–193.
- [20] K.-H. Glassmeier and B. T. Tsurutani, *Hist. Geo Space Sci.* **5**, 11 (2014).
- [21] P. Alken *et al.*, *Earth Planets Space* **73**, 48 (2021).
- [22] E. Friis-Christensen, H. Luhr, and G. Hulot, *Earth Planets Space* **58**, 351 (2006).
- [23] N. Olsen *et al.*, *Earth Planets Space* **65**, 1 (2013).
- [24] See Supplemental Material at <http://link.aps.org/supplemental/10.1103/PhysRevLett.127.101801> for more details of the data analysis, including effects of varying the analysis parameters.
- [25] A. Smith, ESA-VirES/VirES-Python-Client: v0.7.2, <https://doi.org/10.5281/zenodo.4476534>.
- [26] T. Sabaka, L. Tøffner-Clausen, N. Olsen, and C. Finlay, *Earth, Planets Space* **70**, 130 (2018).
- [27] C. C. Finlay, C. Kloss, N. Olsen, M. D. Hammer, L. Tøffner-Clausen, A. Grayver, and A. Kuvshinov, *Earth, Planets Space* **72**, 156 (2020).
- [28] R. T. Birge, *Phys. Rev.* **40**, 207 (1932).
- [29] I. Lira, *Metrologia* **44**, 415 (2007).
- [30] If a significant signal were detected, the variability could also be due to the time evolution of the monopole moment as charged objects are captured by Earth, an effect we neglect in the absence of a signal.
- [31] N. Arkani-Hamed, L. Motl, A. Nicolis, and C. Vafa, *J. High Energy Phys.* **06** (2007) 060.
- [32] B. Hartmann, B. Kleihaus, and J. Kunz, *Phys. Rev. Lett.* **86**, 1422 (2001).
- [33] All magnetic black holes incident on Earth with the large charges and masses considered here will be captured [15].
- [34] E. N. Parker, *Astrophys. J.* **160**, 383 (1970).
- [35] M. S. Turner, E. N. Parker, and T. J. Bogdan, *Phys. Rev. D* **26**, 1296 (1982).
- [36] B. M. Jakosky *et al.*, *Space Sci. Rev.* **195**, 3 (2015).